Geophysical Journal International

Geophys. J. Int. (2014) **197,** 1154–1165
Advance Access publication 2014 March 26

doi: 10.1093/gji/ggu049

Generating regional infrasound celerity-range models using ground-truth information and the implications for event location

Alexandra Nippress,[1] David N. Green,[1] Omar E. Marcillo[2] and Stephen J. Arrowsmith[2]

[1]*AWE Blacknest, Brimpton, Reading,* RG7 4RS, *UK. E-mail: alex@blacknest.gov.uk*
[2]*Los Alamos National Laboratory, NM, USA*

Accepted 2014 February 6. Received 2014 January 22; in original form 2013 August 8

SUMMARY

Celerity-range models, where celerity is defined as the epicentral distance divided by the total traveltime (similar to the definition of group velocity for dispersed seismic surface waves), can be used for the association of infrasound automatic detections, for event location and for the validation of acoustic propagation simulations. Signals recorded from ground truth events are used to establish celerity-range models, but data coverage is uneven in both space and time. To achieve a high density of regional recordings we use data from USArray seismic stations recording air-to-ground coupled waves from explosions during the summers of 2004–2008 at the Utah Training and Test Range, in the western United States, together with data from five microbarograph arrays at regional distances (<1000 km). We have developed a consistent methodology for analysing the infrasound and seismic data, including choosing filter characteristics from a limited group of two-octave wide filter bands and picking the maximum peak-to-peak arrival. We clearly observe tropospheric, thermospheric and stratospheric arrivals, in agreement with regional ray tracing models. Due to data availability and the dependence of infrasound propagation on the season, we develop three regional celerity-range models for the U.S. summer, with a total of 2211 data picks. The new models suggest event locations using the Geiger method could be improved in terms of both accuracy (up to 80 per cent closer to ground truth) and precision (error ellipse area reduced by >90 per cent) when compared to those estimated using the global International Data Center model, particularly for events where stations detect arrivals at ranges <350 km. Whilst adding data-based prior information into the Bayesian Infrasound Source Localization (BISL) method is also shown to increase precision, to increase accuracy, the parameter space must be expanded to include station-specific celerity distributions.

Key words: Probability distributions; Seismic monitoring and test-ban treaty verification; Wave propagation; Acoustic properties; North America.

1 INTRODUCTION

The International Monitoring System (IMS) which is part of the verification measures for a Comprehensive Nuclear-Test-Ban Treaty (CTBT), includes four different sensor networks: seismic, infrasound, hydroacoustic and radionuclide (e.g. Christie & Campus 2010). The planned infrasound network will have 60 stations: 45 are currently installed, with five under development and 10 more planned. Each station comprises an array of at least four microbarometers with apertures between 1 and 4 km, with an average interstation spacing of 2200 km. Thus, whilst this global infrasound network has been shown to be capable of detecting atmospheric explosions with yields of the order of 100 tonnes TNT and greater (Le Pichon *et al.* 2009; Green & Bowers 2010), it is too sparse for constructing regional range-dependent celerity models. Celerity-range models are important because they can be used for the association of automatic infrasound detections, for event location and for the validation of acoustic propagation simulations.

Data from the global IMS network is collected and stored at the International Data Centre (IDC) in Vienna, where observed signals can be used for the association and location of events. As for seismic data, to associate and locate an event with infrasound arrivals, requires traveltime tables or velocity–distance models. However, whilst there are several well accepted global traveltime tables used for seismic signal association and event location, for example, IASP91 (Kennett & Engdahl 1991) and AK135 (Kennett *et al.* 1995), there is currently only one available global traveltime model used for infrasound data (Brachet *et al.* 2010). There are two main

reasons for this difference: (1) the dynamic nature of the atmosphere in comparison to the solid Earth and (2) the small number of infrasound data available, which is a combination of lack of stations and suitable sources. Whilst there are a range of both natural (e.g. volcanoes, bolides, lightning, earthquakes and microbaroms) and man-made (nuclear explosions, chemical explosions and rocket launches) sources of infrasound (Le Pichon *et al.* 2010), to construct a traveltime model requires that these data be 'ground truth'. This means that their location and origin time are known through independent and constrained observations. Furthermore, a large number of recordings of these ground truth events at a range of different distances and azimuths is necessary to provide a high enough data density for the construction of celerity-range models. Unfortunately, such a data density on a global scale does not currently exist. However, infrasound signals are not only recorded by microbarometers; they can also be recorded on seismometers as air-to-ground coupled waves (see e.g. Negraru 2010, and references therein).

Recent studies (e.g. de Groot-Hedlin *et al.* 2008; Walker *et al.* 2011; Hedlin *et al.* 2012) have used data from the seismic US-Array, which provide an unprecedented volume of infrasound signals, particularly for the ground truth repeating source of regular rocket-motor detonations at the Utah Test and Training Range (UTTR), in the western United States. This combination of stations and events provides an ideal opportunity to produce a regional celerity-range model. It should also be noted that in the DTRA Verification database (http://www.rdss.info/) of global infrasound events and data recorded on microbarometer arrays, of the 585 recordings of chemical explosions and mine blasts, 203 are from the UTTR. Therefore any global celerity-range model developed from this database would be biased by the data from the UTTR. An additional source of bias lies in using man-made explosions, as these tend to be conducted during daylight hours only. In our study, all events occur between 16:54 UTC (local time 10:54) and 22:35 UTC (local time 16:35). This bias could influence the observation of for example thermospheric returns, as these have been shown previously to exhibit variations due to semi-diurnal tidal variability in the winds at these high altitudes (>100 km) (Rind 1978). However, we cannot investigate these variations with the data set available.

Infrasound signal characteristics are predominantly controlled by path effects which are a function of the background winds (both speed and direction) and atmospheric temperatures which vary considerably in space and time (Drob *et al.* 2003). These atmospheric variations control which duct (or altitude) the signals are returned from and which azimuth and range observations may be recorded at. For example, the stratospheric winds at altitudes 40–50 km vary seasonally, blowing from east-to-west in the Northern Hemisphere summer months and west-to-east in the winter months (Balachandran *et al.* 1971; Whitaker & Mutschlecner 2008). Therefore, in general, explosions at the UTTR during the summer months produce stratospheric arrivals that are observed to the west of the events at ranges approximately 200 km and greater (e.g. Hedlin *et al.* 2012). In addition to stratospheric arrivals, tropospheric and thermospheric arrivals may also be observed. However, phases propagating within these three distinct atmospheric waveguides are not always easy to distinguish because of their emergent and occasionally overlapping, nature. The celerities associated with each of these phases have bounds which overlap: tropospheric arrivals 0.31–0.33 km s^{-1}, stratospheric 0.28–0.32 km s^{-1} and thermospheric 0.18–0.30 km s^{-1} (Kulichkov 2000), further complicating interpretation.

In this study, a consistent and repeatable method for picking the infrasound arrivals generated by ground truth events at the UTTR is developed and the traveltimes determined are used to calculate celerity. This gives our models internal consistency and allows us to define criteria for which observations are to be used in event location estimation. The different methods for both the infrasound array and seismic data are discussed before presenting the results for celerity versus range. Three different regional celerity-range models for the U.S. Summer are developed and their implications for the location of infrasound events are demonstrated through two different types of location examples. The first location examples use least-squares inversion (Geiger 1912) and are applied firstly to a UTTR event using data from an independent microbarograph array and secondly to an explosion in eastern Europe using data from a dense temporary seismic network, with additional regional seismic stations. The results for the UTTR event clearly show the improvement in both location accuracy and precision from using the new celerity-range models for the U.S. Summer over the current global model. However, whilst the European event highlights that the regional models developed for the western United States are applicable at mid-latitudes in Europe, it also highlights the difficulties of phase identification and the subsequent location problems this can lead to. The second location example uses the same UTTR event, but applies the Bayesian Infrasound Location Technique (BISL) (Modrak *et al.* 2010; Marcillo *et al.* 2014), which provides a mechanism for overcoming the problems of phase identification. The event location is estimated using a uniform prior probability distribution function (pdf), a model-prior pdf based on ray trace modelling (Marcillo *et al.* 2014) and a data-prior pdf based on the celerity-range models presented here.

2 GROUND TRUTH DATA SET

The ground truth information for the explosion events at the UTTR are obtained from the DTRA Verification database (http://www.rdss.info, last accessed 2013 June). This provided a catalogue of 94 events from 2004 to 2008 inclusive. The events occur predominantly in the summer due to the proximity of Salt Lake City ($\sim$100 km east of the UTTR) and associated noise restrictions. The earliest month with data is March and the latest is October (Fig. 1a).

From 2004 to 2008, signals were recorded across five infrasound arrays within 1000 km of the events. These infrasound stations include the IMS stations IS56 (four elements at 860 km range) and IS57 (eight elements at 892 km), along with the following four element arrays: PDIAR (Pinedale Infrasonic Array, Wyoming at 329 km), NVIAR (Nevada Infrasound Array, Mina, Nevada at 552 km) and DLIAR (DOE Prototype Infrasound Array, Los Alamos, New Mexico at 817 km). The majority of the data come from 2006 to 2008 and are recorded on the seismometers of the Transportable Array (TA) of the USArray (Fig. 1b). This array includes over 400 seismometers at $\sim$70 km grid spacing. Thus whilst the rolling nature of the TA from west to east with time (Busby *et al.* 2006) means all stations are not available for all events, combining all the data improves the azimuthal and range coverage significantly.

3 DATA PROCESSING

An important aspect of this study is to use a consistent methodology for determining the traveltime of the infrasound arrivals and to avoid difficulties in phase identification. Because of the multiple emergent phases recorded, the main questions are when to make a pick and

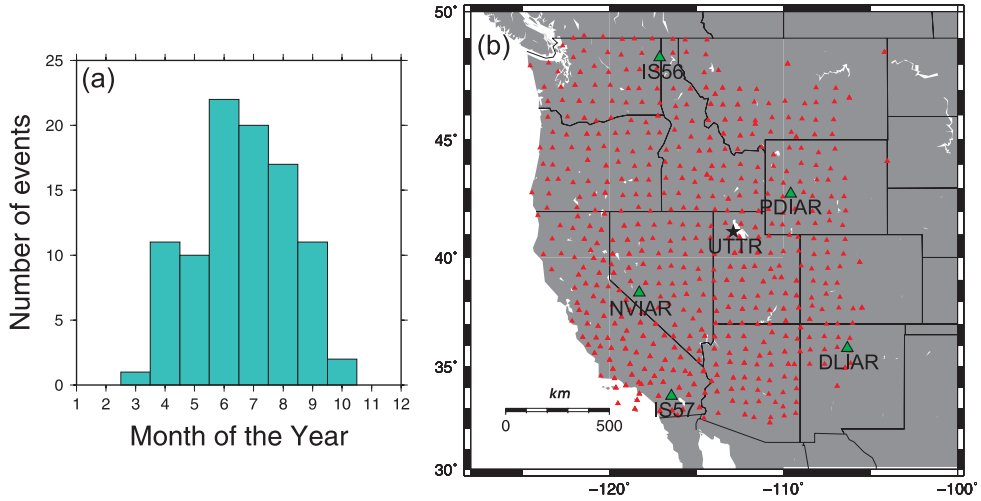

Figure 1. (a) Number of events per month for the years 2004–2008 inclusive. (b) Location of USArray seismic stations (red triangles) and infrasound stations (green triangles) used in this study to detect events at the UTTR (black star). Due to the rolling nature of the USArray from west to east, not all the stations are available for all events.

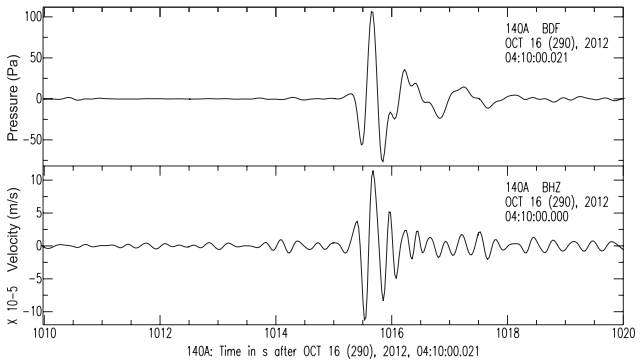

Figure 2. Data for 2012 October 16 explosion at Camp Minden, Louisiana, United States, from USArray station 140A, ∼22 km from the explosion. Both the microbarograph recording (top) and the vertical velocity component of the seismometer (bottom) are bandpass filtered at 1–5 Hz.

which arrival to pick. The answer is to combine these questions and to simply pick the maximum peak-to-peak amplitude arrival irrespective of how many arrivals are observed at a particular station for a single event. This removes the difficulties of picking the onset time in emergent arrivals and allows a pick to be made regardless of the possible phase.

To confirm that maximum peak-to-peak arrival times of infrasound signals recorded on microbarographs are comparable to those of air-to-ground coupled waves recorded on the vertical component of seismometers, an example is taken from the Camp Minden explosion in Louisiana on the 2012 October 16. This event was recorded on the upgraded USArray (TA network), which now has a microbarograph colocated with every seismometer (Vernon *et al.* 2010). Fig. 2 shows an example tropospheric arrival recorded ∼22 km from the explosion and demonstrates that the two-data sets are comparable in terms of the time of peak amplitude.

Although for both data sets the maximum peak-to-peak arrival is used to pick the traveltime and therefore to calculate the celerity given that the epicentral distance is known, the infrasound and seismic data are processed slightly differently because the infrasound stations are arrays whereas the seismic stations are single-instruments.

Table 1. Filters for the infrasound processing are chosen from the following two-octave wide filter bands (e.g. Green & Bowers 2010).

High pass (Hz)	Low pass (Hz)	Window length (s)
0.04	0.16	100
0.08	0.32	50
0.16	0.64	25
0.32	1.28	12.5
0.64	2.56	6.25
1.28	5.12	3.125

3.1 Infrasound recordings

For each event at each array, the pressure channels were beamformed (delayed and summed) over combinations of different backazimuth (true backazimuth ±10° at 1° intervals) and apparent velocity (0.3–0.45 km s^{-1} at 0.005 km s^{-1} intervals). A range of 2-octave band Butterworth 6-pole filters (Table 1; Green & Bowers 2010) were applied to the beamformed data, to find the signal with the maximum *F*-statistic (Blandford 1974). Window lengths were varied to keep the time-bandwidth product constant. This ensures approximately equal data degrees-of-freedom in the different filter bands, allowing *F*-statistic values to be compared across filter bands. The values for azimuth and apparent velocity of the maximum *F*-statistic signal were then used to build the final filtered beam from which the arrival time of the maximum peak-to-peak signal could be picked.

A data example demonstrating these processing steps for NVIAR is shown in Fig. 3. Although in this example there are three signals that can be identified, only one pick is made at the maximum peak-to-peak arrival (the middle arrival in this example). The resulting celerity is 0.31 km s^{-1}, suggesting that this is a stratospheric arrival (see Supporting Information – Infrasound_array_data.xls for a complete table containing all the infrasound recordings processed).

3.2 Seismo-acoustic recordings

Although the seismic stations are part of the USArray, the 70 km spacing is too large to be used as an array for infrasound signals and therefore each station is treated individually. For stations up to ∼60 km away from the UTTR, which are clearly recording high

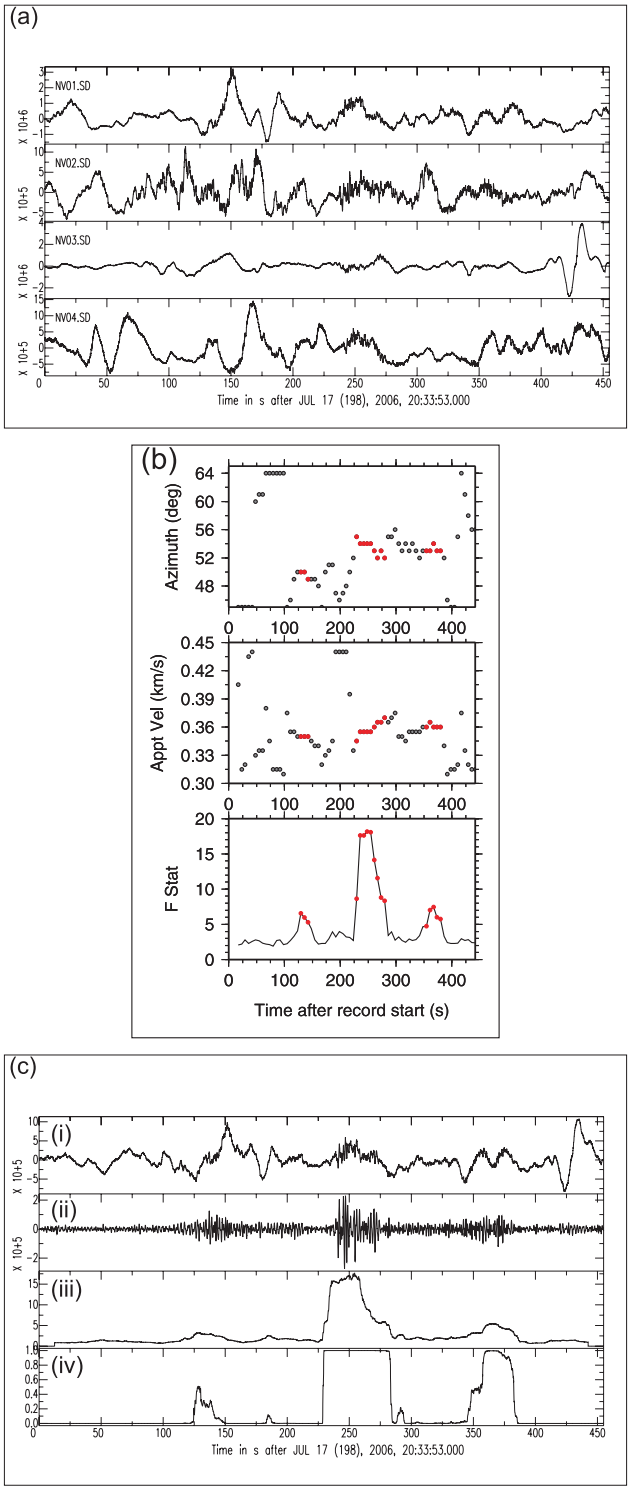

Figure 3. (a) Raw data for a UTTR event recorded on the four-element NVIAR array, 2006 July 17. (b) Beamforming over a combination of back-azimuths and apparent velocities for the NVIAR data shown in part (a). These combinations are for the filter which gave the maximum *F*-statistic: 0.32–1.28 Hz. Red rather than grey circles indicate that the probability of a signal is >95 per cent assuming a signal-to-noise ratio of 1.5. (c) Beam-formed data using the azimuth (54° versus true azimuth 55°) and apparent velocity (0.355 km s^{-1}) combination as determined in part (b). (i) Raw beamed data, (ii) filtered beamed data (0.32–1.28 Hz), (iii) *F*-statistic and (iv) probability assuming an SNR of 1.5. Although three arrivals are observed, only one pick is made at the maximum peak-to-peak on the filtered beam.

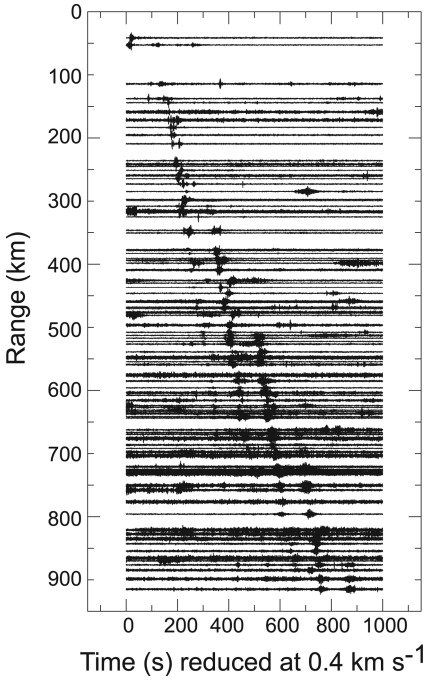

Figure 4. Example data from a UTTR event on 2007 July 16, recorded on the vertical component of the seismometers of the USArray. Data are Butterworth bandpass filtered between 1 and 5 Hz.

frequency tropospheric signals, the data are Butterworth band-pass filtered between 3 and 5 Hz with six poles, with all remaining data filtered between 1 and 5 Hz. The high density of stations allows record sections of the data to be plotted, for example, Fig. 4, which allows clear identification and association of signals to the ground truth event. Following Hedlin *et al.* (2012), times in this figure are reduced at 0.4 km s^{-1}. Again only one pick per station per event is made, for the maximum peak-to-peak arrival (see Supporting Information – Seismic_USArray_data.xls for a complete table containing all the seismic data processed).

4 CELERITY VERSUS RANGE RESULTS

4.1 Celerity-range histograms

The total number of picks for all the available data (infrasound 2004–2008, seismic 2006–2008), with months ranging from April through to October, is 2361. Due to this large number of data points, the results are initially shown as celerity-range histograms and split into four backazimuthal quadrants (north: 315–45°, east: 45–135°, south: 135–225° and west: 225–315°; e.g. Marcillo *et al.* 2014; Fig. 5a). The data are in 50 km range bins and 0.01 km s^{-1} celerity bins. As expected given the dominance of data from the summer, for which the northern hemisphere climatology has the stratospheric winds blowing from east-to-west, the western quadrant has the highest number of arrivals and the east the lowest.

Tropospheric arrivals (celerity > 0.32 km s^{-1}) at ranges between 0 and 150 km (where 150 is the maximum of the bin based on 50 km bins) are observed in all four quadrants. Thermospheric arrivals (celerity < 0.27 km s^{-1}) are only rarely observed, for example, in the northern and eastern quadrants between 250 and 350 km, this is largely due to the lower frequency content (<1 Hz) of thermospheric arrivals, meaning that they are less likely to be observed on a seismometer for which low-frequency noise dominates. The

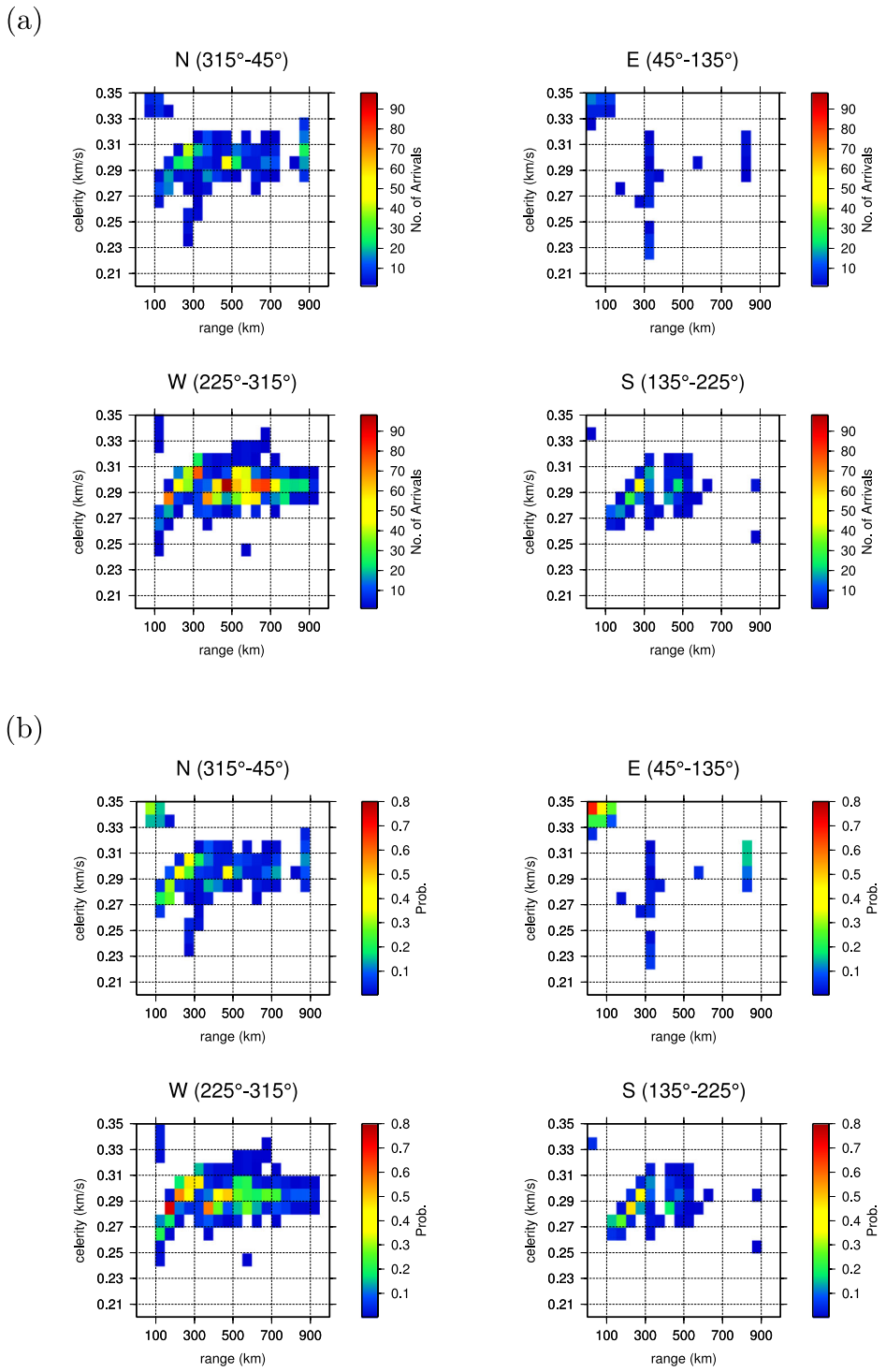

Figure 5. (a) Celerity-range histograms for all data split into four quadrants (backazimuth from the event). Range bins 50 km wide and celerity bins 0.01 km s^{-1} wide. All quadrants have the same colour scale. (b) Probability-based celerity-range histograms for all data split into the same four quadrants as (a) and with the same bin sizes. The probability is the ratio of picks per celerity-range bin to total possible picks per range bin—see text for more details. All quadrants have the same colour scale. It should be noted that for some ranges in particular quadrants, there were no possible picks: north: 0–50 km, east: 850–1000 km, south: 50–100 km and west: 0–100 km.

thermospheric arrivals in the eastern quadrant are predominantly recorded at the Pinedale Array (PDIAR). The highest number of arrivals are stratospheric, with the western, northern and southern quadrants all showing that the arrivals of the first stratospheric branch (i.e. the first ground return) have a steeper gradient in celerity-range than later stratospheric arrivals. It is possible to pick out the second and third stratospheric branches coming in at ∼350 and ∼600 km, respectively, but there is no clear gap between the different branches. When studied in more detail, this overlap between branches shows no simple seasonal pattern. For example, stations at ∼350 km will sometimes have the first stratospheric branch as the maximum peak-to-peak arrival, but for other events, it will be

the second branch. Therefore, through repeated picking of the maximum peak-to-peak arrival time, the aggregated data set provides a probabilistic estimate of which arrival will be observed with maximum amplitude.

To visualize this more clearly, it is necessary to take into account that the data are unevenly distributed in space and time, that is, the number of station-event combinations in a range bin varies between bins. It is the rolling nature of the USArray combined with the geometry of an approximately circular wavefront spreading across a grid from a central point that leads to this discrepancy. However, even if the grid were constant, when comparing bins at different ranges, for example, 0–50 km versus 600–650 km, the further away bin, 600–650 km, would contain more stations because its area is larger. Thus, to account for these uneven distributions, the CRHs are replotted as 'probability' CRHs, with a scale that is the ratio of the number of arrivals picked per celerity-range bin to the number of possible arrivals for that range bin (Fig. 5b), rather than simply the number of arrivals picked in a particular 50 km by 0.01 km s^{-1} bin. The number of possible arrivals in a given range bin is the sum of all the station-event combinations in that range bin.

Comparing Figs 5(a) and (b), it can be seen that for part (a) the largest number of arrivals is at 450–500 km in the western quadrant (it is not at ∼1000 km because beyond around 600 km, it gets increasingly difficult to observe air-to-ground couple waves), whereas for part (b), the highest probability is at 150–200 km in the western quadrant. Furthermore, the original CRHs suggested only a small number of tropospheric observations in the eastern quadrant, but the implication of the probability CRH is that if stations are available then a tropospheric observation to the east is more likely than in any other quadrant. As expected the western quadrant still dominates, but the emphasis has now shifted to the first and then second stratospheric branch. It is also easier to observe that the thermospheric arrivals in the northern quadrant are unusual and are in fact down to just one event.

Although the CRHs are a useful visualization tool and may be used for comparing data-based results with model-based results (Marcillo *et al.* 2014), to develop a celerity-range model to be used for event location, we use the individual arrival picks and their associated celerities.

4.2 Summer celerity-range models

As discussed in Section 2 and shown in Fig. 1(a), the majority of the data are from the summer months. Given the well known seasonal variations in infrasound propagation, we choose to construct a model only applicable to summer months. To determine which time period to use for the summer model, the effective sound speed profile and effective sound speed ratio (when compared to the ground surface) from the HWM07 climatological model (wind; Drob *et al.* 2008) and the MSISE-00 model (temperature; Hedin 1991) for the westerly direction from the UTTR event location over the period of one year are used. From these models, the time period with a dominant stratospheric acoustic duct is taken to be when the effective sound speed ratio is ≥1, which is from mid-May to the end of August, with April and September being transitionary periods between the dominant easterly winds (summer) to the dominant westerly winds (winter). Using these dates, only 6 per cent of the total data are not used (see Supporting Information – summer_celerity data.txt for a table of the summer celerity-range data used). The main difference between plots of CRHs using the summer data only versus those for all the data as shown in Fig. 5 is that there are fewer stratospheric arrivals in the eastern quadrant during the summer only.

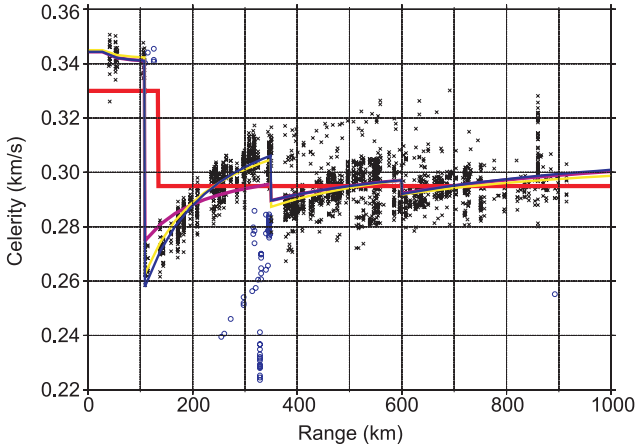

Figure 6. Celerity versus range plot of all available summer data at all backazimuths (black crosses and blue circles, with blue circles indicating data that have been removed to generate the edited model—see text for further details). The three new range-dependent celerity models for the U.S. Summer are shown: All summer data model (magenta line), Edited data model (blue line) and Weighted data model (yellow line), with the global IDC range-dependent celerity model also shown for comparison (Brachet *et al.* 2010) (red line).

The dominance of arrivals in the western quadrant for the summer time period, together with the similarities between the northern, southern and western quadrants, leads us to develop an azimuthally independent regional celerity-range model. This choice also simplifies the application of the model in location codes. Fig. 6 shows all the summer celerity-range data from all backazimuths and again highlights that there are different phases arriving at different ranges, but with overlap between the phases. This overlap complicates the construction of a simple regional celerity-range model and therefore three different models are developed (see Supporting Information – TTmodel_table.txt for the traveltime tables of all three models). For each of these models, we split the range from 0 to 1000 km into four sections based on the density of data and the probability CRHs which show which arrivals are most likely to be observed at a particular range. The first section from 0 to 110 km is the tropospheric part of the model, the second from 110 to 350 km is the first stratospheric branch, 350–600 km is the second stratospheric branch and from 600 to 1000 km is for the third and later stratospheric branches.

For each model, we use a linear least-squares regression to predict traveltimes as a function of range in each of the four range sections (Table 2) and use the 95 per cent confidence limits on this regression to provide errors on the model. The 95 per cent confidence limits are calculated using the MATLAB polyval function, which estimates the standard deviation of the error in predicting a future observation, which in this example is the traveltime at a given range (see Supporting Information – figureS.1.pdf for a figure showing the picked traveltimes and the linear fits). The difference between the models is because we vary the input data. Thus, the first model includes all the summer data (Fig. 6, magenta line) and we will refer to this as the 'all data' model. This model fits the tropospheric, second branch stratospheric and later stratospheric branches well. However, it is clearly influenced by longer range tropospheric and thermospheric arrivals, meaning that it does not capture the celerity-range gradient for the first stratospheric branch very well, for example, it tends to lower celerities than the majority of the data suggest, at ranges 250–350 km. Furthermore, it can be seen in Fig. 7(c). that the errors for the first stratospheric branch are very large, particularly where there is overlap between the

Table 2. The coefficients for the traveltime linear regression analysis for each range section (Tropospheric, Tropo.; Stratospheric branches, Strat. 1st, 2nd and 3rd plus later branches) of each new regional model. The equation is of the form $y = mx + c$ where y is the traveltime (s), m is the gradient, x is the range (in degrees) and c is the y-intercept.

	Tropo. 0–110 km		Strat. 1st 110–350 km		Strat. 2nd 350–600 km		Strat. 3rd plus 600–1000 km	
Model	m	c	m	c	m	c	m	c
All data	327.04	−1.05	363.02	40.85	360.59	73.54	354.81	138.43
Edited data	327.04	−1.05	332.29	96.93	360.59	73.54	352.59	151.89
Weighted data	325.65	−0.83	338.42	83.29	356.24	96.86	358.86	119.69

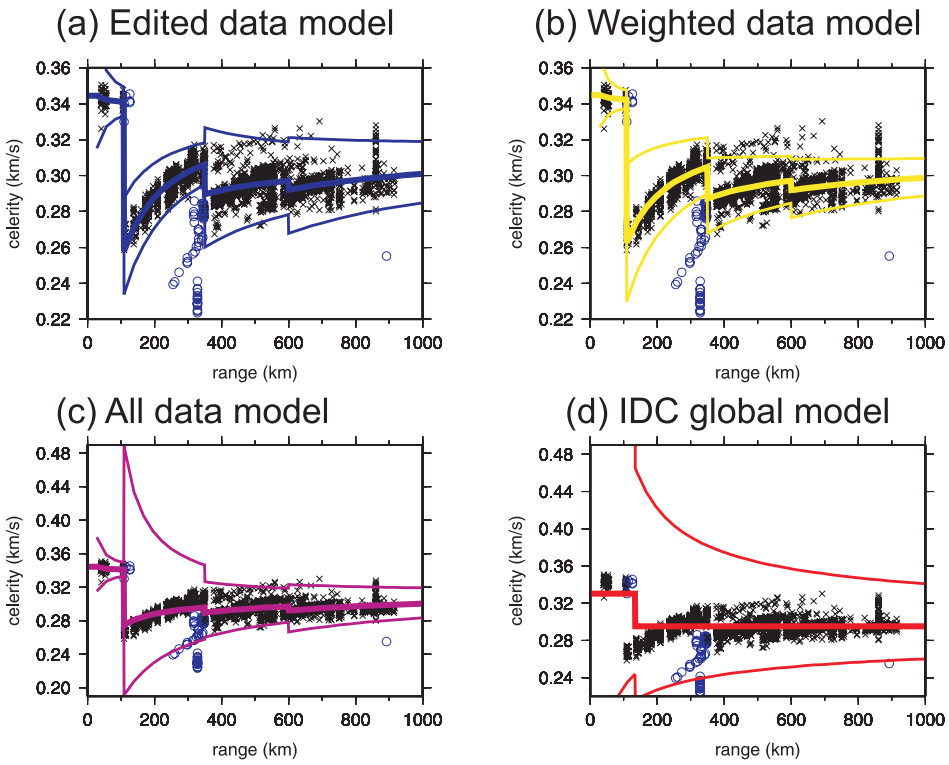

Figure 7. Individual model celerity-range plots, with 95 per cent error bounds shown. Data and models colours are the same as in Fig. 6. Note that the edited and weighted data models have a different scale to the all data model and IDC global model (Brachet *et al.* 2010).

tropospheric and first stratospheric branch arrivals in the data at around 110 km. Currently no constraint is placed on the allowed values of celerity, therefore unphysical celerities are contained within these confidence limits.

To account for the lack of good fit to the first stratospheric branch for the all data model, two further models are developed. The first of which is the edited model. For this model, using the probability CRHs as a guide as to which arrivals are more likely at a particular range, the following arrivals are removed: tropospheric beyond 110 km (celerity $> 0.32\,\mathrm{km\,s^{-1}}$), all thermospheric arrivals (arrivals with celerity $< 0.28\,\mathrm{km\,s^{-1}}$) and the earliest arriving second stratospheric branch data (Fig. 6). The single observation at thermospheric celerity at ∼800 km range is also removed. This edited model (Fig. 6, blue line) is the same as the all data model in range sections one (tropospheric) and three (second stratospheric branch), very similar in section four (third and later stratospheric branches), but now fits the stratospheric first branch data with much tighter confidence limits than the all data model (Fig. 7a).

The final model is a 'weighted-model'. This time rather than subjectively removing data, the probabilities from the probability CRHs are used to weight data from each celerity-range bin ($B_{c,r}$). For each range bin (B_r), we normalize using the celerity-range bin with the maximum probability to remove bias in weight between different range bins. Therefore, the maximum possible weight is 1 and the weights (W) for a given celerity (c_d) and range (r_d) are calculated as follows:

$$W(c_d, r_d) = \frac{P(B_{c_d,r_d})}{P_{\max}(B_{c,r_d})}, \tag{1}$$

where

$$P(B_{c,r}) = \frac{\text{number of picks in } B_{c,r}}{\text{number of possible picks in } B_r}. \tag{2}$$

The resulting model is very similar to the edited model as we would expect (Fig. 6, yellow line), but the confidence limits are now larger again for the first stratospheric branch (although not as large as for the all data model), but tighter for the later stratospheric branches (Fig. 7b). It should be noted for all three regional models, that the closest station for which data are available is at ∼40 km, therefore the models are not well constrained for smaller ranges (Figs 7a–c).

The global-celerity-range model used at the IDC is also shown for comparison in Fig. 6. Whilst at ranges beyond ∼400 km, the new models and the IDC model are very similar, it is clear that particularly between 110 and 350 km, the global model is not capturing the variation in celerity with range that is shown in the regional data. Furthermore, the IDC model is underestimating the celerity of the tropospheric arrivals for this region. The traveltime modelling errors for the IDC model are also a function of range with degrees and are defined empirically (Brachet *et al.* 2010). However, for tropospheric arrivals, the modelling error is unphysical (Fig. 7d).

The implications for infrasound location of these new models is now investigated through a range of different examples.

5 IMPLICATIONS FOR INFRASOUND LOCATIONS

The implications for event location accuracy and precision of this celerity-range data set and the three different regional models derived from it, are explored using two different techniques. The first, uses the Geiger (1912) method (an iterative least-squares technique, which minimizes the traveltime residual between the arrival time observed at each station and that predicted by the trial event location) to determine what improvement if any can be gained through using the regional models. For a recent discussion of the Geiger method, see for example, Douglas (2013). The second, uses the BISL method (Modrak *et al.* 2010), to compare location results using a model-based prior probability density function (pdf) with those using a data-based prior pdf.

Although it is common to use both arrival time and azimuth observations as input to location techniques, the examples presented here all use arrival time observations only. This is because for the following examples, the majority of the stations used are single instruments and an array is required if the backazimuth is to be measured. Furthermore, whilst the backazimuth for each infrasound array observation was recorded (see Supporting Information – Infrasound_array_data.xls), the number of recordings are not sufficient to develop a model for the backazimuth deviation (the difference between the observed and true backazimuth), that could be used to provide uncertainties on the backazimuth observations.

The new models have all been developed using data from the summer in the mid-latitudes of the western United States, therefore, the first and most appropriate test is to locate an event in this region at this time of year. Furthermore, for comparing the location found using the new regional models versus the IDC global model, it is important to have stations at ranges <350 km from the event because this is the range where the models show the largest differences. To test whether this regional model is applicable to other mid-latitude regions in the summer, an event from Europe is also located. For the model versus data pdf comparison using the BISL technique, the same western U.S. example event is used.

5.1 UTTR event, 2007 August 6, Utah, United States

This event was one of the many UTTR events used to build the celerity-range data set. However, the data to be used for this location estimate are from an independent network and are not used to generate the models. The data are from a temporary infrasound network (Stump *et al.* 2007) with a mixture of arrays (three) and individual stations (14) (Fig. 8). Originally the network was to be used as part of the Divine Strake experiment, but following its cancellation, the network was operational throughout 2007 August to monitor explosions at the UTTR. The stations range from <1 to

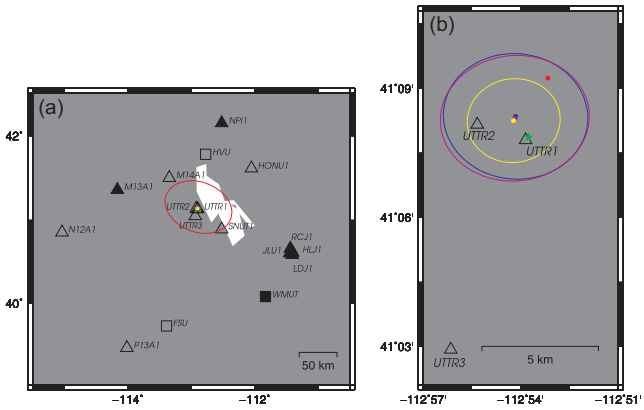

Figure 8. Locating the 2007 August 6 UTTR event. (a) Temporary infrasound network location map with arrays (squares) and single instruments (triangles). Stations with picks (open symbols), without picks (filled symbols) along with the event location (green star) and 95 per cent confidence error ellipes are shown. Model colours are the same as in Fig. 6. (b) Zoomed in map of the event locations and error ellipses.

∼210 km away, sampling the tropospheric and stratospheric first branch sections of the regional celerity-range models. The network also included a small number of colocated seismometers, but only the infrasound recordings are used for this location.

The infrasound data are processed as described in Section 3, with picks made at the time of the maximum peak-to-peak arrival. Arrivals were observed at 10 of the 17 possible stations. The location code uses the Geiger (1912) method and the results are shown in Fig. 8. From this figure, it can be clearly seen that all three regional models have improved location accuracy (proximity to ground truth) when compared to the global model location (shown in red). Distances from ground truth are: all data—1.0 km, edited data—1.1 km, weighted data—1.0 km versus 2.7 km for the global model. Furthermore, due to the smaller errors on the regional models in comparison to the global model, the precision of the location results is also improved as shown by the smaller error ellipses for the regional models (all data—27 km^2, edited data—26 km^2, weighted data—11 km^2 versus 4703 km^2 for the global model). The size and shape of the error ellipse depends on the uncertainties in arrival time measurements, the number and geographic distribution of the stations used and the errors in the celerity-range model. It should be noted that only the model is varied for each location estimate, the stations and associated observational uncertainties are the same and therefore it is the model errors that are controlling the differences in error ellipse.

Although only one UTTR event is shown, we repeated this process for the three other events during 2007 August and the results all agree, with the regional models producing more accurate and higher precision locations than the global model. The improvement in accuracy ranges from a maximum of 80 per cent to a minimum of 50 per cent, whilst the error ellipses for the regional models are consistently <1 per cent of the size of the global IDC model error ellipse. In addition to the improvements in location, the average difference in origin time for all three regional models for the four events and the ground truth origin time is 1.7 s, whereas for the global model, the difference is 3.2 s.

5.2 Chelopechene explosion, 2008 July 3, Bulgaria

To test whether the new regional models are applicable to other regions at similar latitudes during the summer, a ground-truth event

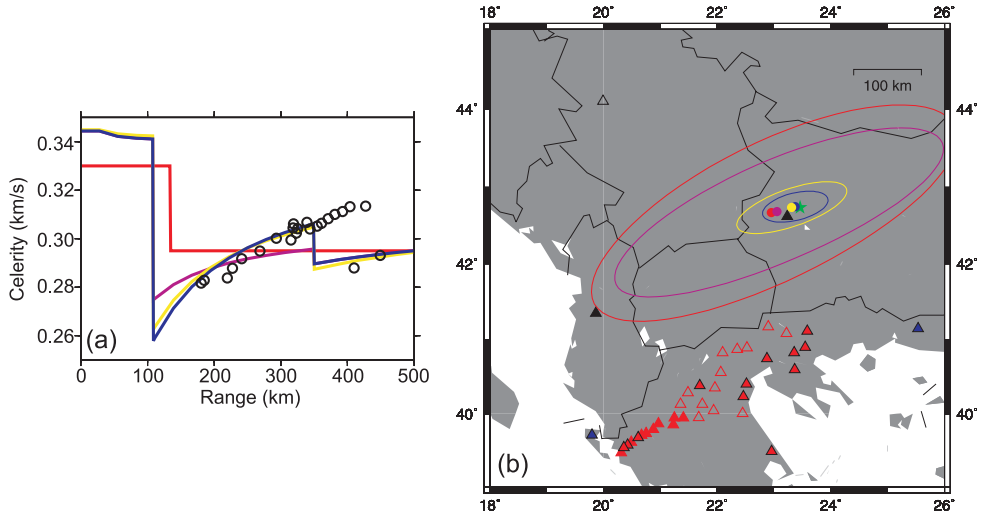

Figure 9. Locating the Chelopechene 2008 July 3 event. (a) Celerity-range plot showing all the picks for this event (black circles), with the three new regional models and the global model. Model colours are the same as in Fig. 6. (b) Network and event location (green star) map. Stations with picks (open triangles), stations with no picks (filled triangles). The event location and error ellipses are shown. Model colours are the same as in Fig. 6. The following networks had stations within 1000 km and had picks—MN, MEDNET project, Instituto Nazionale di Geofisica e Vulacnolgia, Rome, Italy, (black triangles) and XS2008, MEDUSA project (see text), (red triangles). For the XS2008 network, stations beyond 350 km that had picks removed for the location results to converge are shown as filled red triangles. Those stations that had no pick are shown as filled red triangles with a black outline. The HL, National Observatory of Athens Digital Broadband Network, Greece, (blue triangles) had stations within 1000 km and within the mapped area, but no picks. The following networks had stations within 1000 km but had no picks and are outside the mapped area—GE, GEOFON program: GFZ Potsdam, Germany, RO, Romanian Seismic Network: National Institute for Earth Physics, PL, Polish Seismological Network: Polish Academy of Sciences and IU, Global Seismograph Network: GSN—IRIS/USGS.

with sufficient regional station coverage is required. Although regional infrasound networks are uncommon, regional seismic networks are extensively deployed. In 2008, a series of accidental explosions occurred at an arms depot in Chelopechene, Bulgaria (Green *et al.* 2011). Here we study arrivals generated by the largest explosion (origin time 2008 July 3 03:31:13 ± 5 and an equivalent chemical yield of the order of 100 t) recorded on a dense temporary network of seismic stations installed in Greece as part of the MEDUSA project (e.g. Suckale *et al.* 2009). These stations, along with additional regional network stations provided sufficient data coverage to determine a location.

The station-to-source distance for stations where an arrival was picked ranges from 180 to 450 km. Unfortunately, the closest seismometer (VTS – MEDNET Project station) ∼22 km from the event, is too close for an infrasound arrival to be observed within the seismic arrivals. This means that the stations with picks are sampling the first and second branch stratospheric arrivals only.

The seismic data are processed following the criteria set out in Section 3, but the location results do not converge for the regional models. Looking at the data, it is straightforward to explain why. For this event, the maximum peak-to-peak arrival continues to be the first branch stratospheric, beyond 350 km (Fig. 9a). Therefore, because at these distances the regional models predict second stratospheric branch arrivals, none of them can fit the data beyond 350 km well enough for the results to converge. This highlights the problem of phase identification or rather mis-identification. It is only because of the dense network available in this example that this behaviour can be observed; it is not always straightforward to tell whether an arrival is a first or second branch arrival. If the location is rerun using only stations at ranges <350 km, then as for the UTTR events, all three models show improved accuracy (distance to ground truth, all data—34 km, edited data—7 km, weighted data—12 km, global model—42 km) and precision (area of error ellipse, all data—58 460 km^2, edited data—2981 km^2, weighted data—7053 km^2, global model—90 517 km^2) when compared to the results for the global model (Fig. 9b). Here, even for this non-ideal case, the weighted model error ellipse area is >90 per cent smaller than the IDC model's. The relatively poor performance of the all data model this time as opposed to for UTTR is due to the lack of additional stations at tropospheric ranges. The regional models also have smaller differences between their origin time results and ground truth origin time (all data—42 s, edited data—12 s, weighted data—20 s) than the global model (65 s).

Producing models that account for the behaviour observed for the Chelopechene event is complicated. The ideal solution is to be able to include phase information with the pick time, however, as already discussed, this is not always possible. An alternative is to have an adaptive location algorithm that will try different models if the residuals are high, for example, if the model for the first stratospheric branch was extrapolated beyond 350 km. The difficulty with this is how to define which arrivals should be used for the first branch model and which are actually fast arriving second branch signals.

Taking all these factors into account suggests an alternative approach may be required. The BISL approach has been introduced in detail elsewhere (Modrak *et al.* 2010) and most recently has been adapted to include prior pdfs for the celerity-range distribution based on results from ray trace modelling (Marcillo *et al.* 2014). Currently, due to computational expense, only a network prior pdf may be used; which is the average of all the station-specific prior pdfs for the network. Although this limits the potential advantages of such a technique, it has already been shown to provide improvements in precision over uniform priors. We will now compare the results of using data-based prior pdfs with model-based prior pdfs for the UTTR event located in Section 5.1.

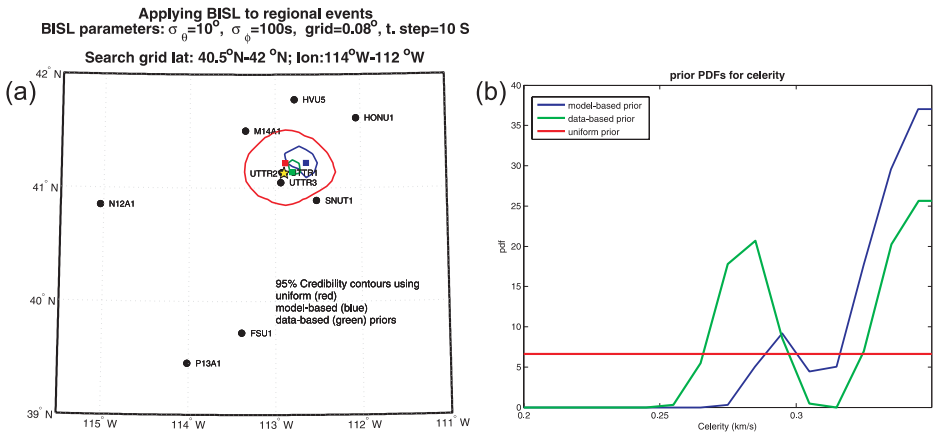

Figure 10. Locating the 2007 August 6 UTTR event using the BISL technique and three different network-average prior pdfs, uniform, model CRH-based and data CRH-based. (a) Temporary infrasound network location map (black dots), 95 per cent credibility contours using uniform (red), model CRH-based (blue) and data CRH-based (green) priors, with their maximum *a posteriori* (MAP) points shown as squares. Ground truth (yellow star). (b) Prior pdfs corresponding to the MAP point for the event location. Uniform (red), model CRH-based (blue) and data CRH-based (green).

5.3 BISL location—UTTR event, 2007 August 6, Utah, United States

The BISL method estimates the most likely source location given a set of arrival times and/or backazimuths by performing a grid search over a 4-D parameter space which includes the two horizontal coordinates, celerity and origin time (Modrak *et al.* 2010). The difference between the model (obtained by evaluating the parameter space) and measured backazimuths and arrival times, are used to build a probability distribution (likelihood pdf). Following the Bayesian methodology, a posterior pdf is built by combining prior information (which may be used to further constrain the parameter space), with the likelihood pdf. Higher values in the posterior pdf are considered the most likely solution. A key advantage of BISL is its flexibility; any probability distribution can be used as appropriate and prior constraints can readily be folded into the solution. The original work of Modrak *et al.* (2010) used uniform-value priors for celerity-range, whereas the recent study of Marcillo *et al.* (2014) shows that the precision of locations can be improved by using enhanced priors based on CRHs generated using ray tracing propagation catalogs. Here we compare the location results for the 2007 August 6, UTTR event (Section 5.1), using a uniform prior pdf, a model CRH-based prior pdf and a new data CRH-based prior pdf. For a more detailed explanation of the BISL technique, see Modrak *et al.* (2010) and Marcillo *et al.* (2014).

The data CRH-based prior pdfs are taken from the probability CRHs for each backazimuth quadrant for summer only data. The network pdf used for the BISL location is an average of the pdfs for each of the 10 stations where arrivals were observed (Fig. 10 b). The results (Fig. 10a) clearly show the improvement in precision of the model CRH-based prior pdf (area of 95 per cent credibility contour 781.8 km^2) over the uniform prior pdf (area 6302.9 km^2), consistent with the previous results of Marcillo *et al.* (2014), in addition to a further improvement in precision when implementing the data CRH-based prior pdf (area 165.7 km^2). Implementing CRH-based priors instead of the uniform prior, assigns higher probabilities of occurrence to more realistic celerity distributions, thus increasing the precision of the location algorithm. For this example, the data-based CRH prior pdf increases the precision over the model-based CRH prior pdf, because the model-based CRH prior pdf overestimates the celerity of the stratospheric arrivals (which are observed at FSU1 (range 162 km), N12A1 (range 182 km) and P13A1 (range 209 km), whilst underestimating the probability of seeing statospheric arrivals. This is due to the limitations of ray tracing modelling, where first stratospheric bounce arrivals are rarely observed closer than ∼200 km. The remaining seven stations (ranges $\leq$ 89 km) all observe tropospheric arrivals and it is these arrivals that dominate both the model-based and data-based CRH prior pdfs (Fig. 10b). These higher celerity values, when applied to the 'stratospheric' stations, cause the credibility contours of both the model-based and data-based prior pdfs to be biased to the northeast of ground truth, as the location algorithm has to increase the range to these stations to minimize the difference between the observed and predicted traveltimes.

Although the precision has been improved and the maximum *a posteriori* (MAP) point for the data-based CRH is closer to ground truth than the uniform prior MAP point, the accuracy of the event location for both the data-based CRH prior and model-based CRH prior are unacceptable because their 95 per cent credibility contours do not include the ground truth location. This improvement in precision but not accuracy was also observed by Marcillo *et al.* (2014) and highlights the weakness in using a network average prior over station-specific priors in the BISL methodology. Incorporating station-specific priors is computationally expensive; each station adds another dimension to the matrix of posterior pdf values that must be constructed. Efficient solutions for station-specific priors is the focus of our ongoing research, as they will lead to an increase in both location accuracy and precision. For example, with the Chelopechene event location in the previous section, the celerity-range model has only one celerity value beyond 350 km, whereas a station specific data-based CRH for stations beyond this range would allow a range of celerities with different probabilities to be used for the location, therefore removing or at least reducing the difficulties of phase identification.

6 DISCUSSION

The celerity-range results presented here for data recorded across the USArray and additional infrasound arrays for 2004–2008 inclusive (Figs 5 and 6), show very good agreement with a previous study of infrasound signals for 2007 (Hedlin *et al.* 2012). Although the processing techniques differ (we used slightly different filters and picked the maximum peak-to-peak arrival only), both studies observe tropospheric arrivals, along with up to four stratospheric arrival branches, in addition to observing 1st branch stratospheric

arrivals within the geometric shadow zone as defined by ray tracing models. Furthermore, as the distance from the source increases, the vertical distance travelled (from the source to the turning point and back to the ground), becomes a less important contributor to traveltime and thus the celerity of each branch increases with range (Hedlin *et al.* 2012).

Although the new regional models are defined for the summer only, the data still show a range of celerities at any particular distance from the event (Fig. 6). In general, as observed in previous studies (e.g. Che *et al.* 2011; Hedlin *et al.* 2012), the celerity increases from early through to mid-summer, before decreasing again. However, due to the variability of the atmosphere, this variation is not a smooth continuous curve and waveforms may vary significantly even for a series of identical sources at the same location but separated by hours or days and recorded by the same stations (e.g. Kulichkov & Bush 2001).

This study complements an earlier study by Che *et al.* (2011), in South Korea, which produced seasonally dependent celerity models for two infrasound stations, using over 1000 repeating events, over 2 yr. They showed that these regional models produced improved event locations and it is interesting to note that the range of celerities observed for their station CHNAR from mid-May to August (traveltimes of 625–670 s corresponding to celerities between 0.27 and 0.29 km s^{-1}) agrees very well with the range of celerities observed at the same range (181 km) for the data from the UTTR. These results provide further evidence alongside the Chelopechene event (Fig. 9), that our regional models developed from data recorded in the western United States, may be applicable to Northern Hemisphere mid-latitudes in all continental regions. It should be noted however, that these comparisons are largely restricted to the first stratospheric branch. In the South Korean study (Che *et al.* 2011), tropospheric signals are observed to the east of the events at 169 km distance, almost 40 km further than they are observed for the UTTR when picking the maximum peak-to-peak arrivals. However, the South Korean tropospheric path is dominated by open ocean, whereas the UTTR paths are all continental. This leads us to tentatively suggest that models for tropospheric arrivals whilst less seasonally specific, may be more regionally specific, whereas stratospheric models may be appropriate for specific latitudinal bands and seasons.

Although the suggestion that the model is applicable to other Northern Hemisphere mid-latitude regions is encouraging, the spatial variability of atmospheric fluctuations do not allow this model to be used globally. Due to the sparse nature of global infrasound networks, it is currently unlikely that detailed data-driven celerity models as constructed in this paper will become available worldwide. Therefore, it is likely that future global celerity models will be generated using numerical acoustic propagation modelling techniques with appropriate meteorological specifications [recent comparisons of model and data celerity values include: Ceranna *et al.* (2009), Che *et al.* (2011) and Assink *et al.* (2012)]. Such modelling techniques will allow updateable, region and time specific models to be generated, but require validation against high quality data sets, such as the one presented in this paper.

For the event location examples presented in Section 5, only arrival time observations were used. Backazimuth data were not utilized, because there is not sufficient infrasound array data within the UTTR data set to constrain a backazimuth deviation model; most of the stations used were single seismometer installations. However, it is often the case that acoustic events are recorded across a low number of stations within a sparse infrasound monitoring network, such as the 60 station global infrasound array network of the IMS. Therefore, we investigated the effects on location accuracy and precision of including azimuth observations for the three UTTR events detailed in Section 5.1 for which arrivals were recorded at three arrays.

When azimuths from the three arrays are added to all available arrival times (minimum number of times is 11), the additional location constraints are small. The location estimates vary by less than 1 km , hence the accuracy is almost unaffected. The effect on the error ellipse, and therefore precision, is controlled by the bias on the backazimuth measurements. Because the measurements are made in the U.S. summertime, the prevailing westward stratospheric winds generate backazimuth deviations towards the west. Because this bias is unaccounted for in our models, error ellipses tend to elongate along an east–west axis reducing precision in all cases except where arrival times are consistent with a source located to the west of ground truth.

When location estimates are made using arrival time and azimuth data from just the three arrays, the backazimuth estimate bias due to the effect of the stratospheric winds has an increasingly large effect. Therefore, location estimates consistently fall to the west of ground truth. To reduce this effect, significantly more infrasound array data will be required to validate predictive models for backazimuth deviations.

7 CONCLUDING REMARKS

Recordings of 94 events at the UTTR, western United States, during the summer months on the USArray seismometers, supplemented with available infrasound array data, have allowed us to collate over 2300 infrasound arrival observations. We have developed a consistent set of criteria for processing both sets of data to provide traveltimes which can be presented as range-dependent celerity observations. From these observations, we have developed three new regional celerity-range models for the U.S. summer, which are applicable to surface disturbances only (they are not applicable to events at altitude, e.g. meteorite explosions). These have been shown to potentially improve both the accuracy (e.g. by up to 3.9 km for events at the UTTR) and precision (error ellipses reduced by 99 per cent for events at the UTTR) of infrasound locations over currently used global models. Our preferred new model is the weighted model because it shows greater improvement in both accuracy and precision than the all data model and unlike the edited model, it takes into account how likely a celerity-range observation is through the probability CRH used for the weighting, rather than having this choice made subjectively. The improvements to location for each new model depend on two crucial factors: (1) the range over which the observations are made and (2) the atmospheric conditions on the day of the event. For example when the Chelopechene event is located, the stratospheric first branch arrivals extend beyond the 350 km limit for this type of arrival in the new regional models, meaning that these models cannot converge on a result. However, if the observational range is restricted to stations $<$350 km, then the new regional models provide improved location over the global model. This difficulty with phase identification, leads us to suggest that Bayesian algorithms implementing station-specific celerity prior pdfs should be the focus of future work for location.

ACKNOWLEDGEMENTS

OEM and SJA acknowledge the support of Leslie Casey and the National Nuclear Security Administration Office of Nonproliferation and Treaty Verification Research and Development for funding this work. Los Alamos National Laboratory completed this work under the auspices of the U.S. Department of Energy under contract

DE-AC52-06NA24596. We thank the IRIS (Incorporated Research Institutions for Seismology) DMC for the availability of data used for the UTTR and Chelopechene locations and the Camp Minden explosion comparison. More information on the networks that collected these data are available at: http://www.fdsn.org/citation.htm. The TA network data from the USArray are freely available as part of the EarthScope USArray facility, operated by IRIS and supported by the National Science Foundation, under Cooperative Agreements EAR-0323309, EAR-0323311, EAR-0733069. Figures prepared using GMT (Wessel & Smith 1998). We thank two anonymous reviewers for comments which improved this paper.

REFERENCES

Assink, J.D., Waxler, R. & Drob, D., 2012. On the sensitivity of infrasonic traveltimes in the equatorial region to the atmospheric tides, *J. geophys. Res.,* **117**(D01110), doi:10.1029/2011JD016107.

Balachandran, N.K., Donn, W.J. & Kaschak, G., 1971. On the propagation of infrasound from rockets: effects of winds, *J. acoust. Soc. Am.,* **50**(2), 397–404.

Blandford, R.R., 1974. An automatic event detector at the Tonto Forest Seismic Observatory, *Geophysics,* **39**(5), 633–643.

Brachet, N., Brown, D., Le Bras, R., Mialle, P. & Coyne, J., 2010. Monitoring the Earth's atmosphere with the Global IMS Infrasound Network, in *Infrasound Monitoring for Atmospheric Studies,* pp. 77–118, eds, Le Pichon, A., Blanc, E. & Hauchecorne, A. Springer.

Busby, R.W., Vernon, F.L., Newman, R.L. & Astiz, L., 2006. Earth-Scope's USArray: advancing eastward, *EOS Trans. Am. geophys. Un.,* **87**(52), Fall Meet. Suppl., Abstract U41B-0820.

Ceranna, L., Le Pichon, A., Green, D.N. & Mialle, P., 2009. The Buncefield Explosion: a benchmark for infrasound analysis across Central Europe, *Geophys. J. Int.,* **177**(2), 491–508.

Che, I-Y., Stump, B.W. & Lee, H-I., 2011. Experimental characterization of seasonal variations in infrasonic traveltimes on the Korean Peninsula with implications for infrasound event location, *Geophys. J. Int.,* **185,** 190–200.

Christie, D.R. & Campus, P., 2010. The IMS Infrasound Network: design and establishment of infrasound stations, in *Infrasound Monitoring for Atmospheric Studies,* pp. 29–75, eds, Le Pichon, A., Blanc, E. & Hauchecorne, A. Springer.

de Groot-Hedlin, C., Hedlin, M.A.H., Walker, K.T., Drob, D.P. & Zumberge, M.A., 2008. Evaluation of infrasound signals from the Shuttle Atlantis using a large seismic network, *J. acoust. Soc. Am.,* **124**(3), 1442–1451.

Douglas, A., 2013. *Forensic Seismology and Nuclear Test Bans,* pp. 56–58. Cambridge Univ. Press.

Drob, D.P., Picone, J.M. & Garces, M., 2003. Global morphology of infrasound propagation, *J. geophys. Res.,* **108**(D21), 4680.

Drob, D.P. *et al.*, 2008. An empirical model of the Earth's horizontal wind fields: HWM07, *J. geophys. Res.,* **113**(A12304), doi:10.1029/2008JA013668.

Geiger, L., 1912. Probability method for the determination of earthquake epicenters from the arrival time only, *Bull. St. Louis Univ.,* **8,** 60–71.

Green, D.N. & Bowers, D., 2010. Estimating the detection capability of the International Monitoring System Infrasound Network, *J. geophys. Res.,* **115**(D18116), doi:10.1029/2010JD014017.

Green, D.N., Vergoz, J., Gibson, R., Le Pichon, A. & Ceranna, L., 2011. Infrasound radiated by the Gerdec and Chelopechene explosions: propagation along unexpected paths, *Geophys. J. Int.,* **185**(2), 890–910.

Hedin, A.E., 1991. Extension of the MSIS thermosphere model into the middle and lower atmosphere, *J. geophys. Res. Space Physics,* **96**(A2), 1159–1172.

Hedlin, M.A.H., de Groot-Hedlin, C. & Drob, D., 2012. A study of infrasound propagation using dense seismic network recordings of surface explosions, *Bull. seism. Soc. Am.,* **102**(5), 1927–1937.

Kennett, B.L.N. & Engdahl, E.R., 1991. Travel times for global earthquake location and phase association, *Geophys. J. Int.,* **105,** 429–465.

Kennett, B.L.N., Engdahl, E.R. & Buland, R., 1995. Constraints on seismic velocities in the Earth from travel times, *Geophys. J. Int.,* **122,** 108–124.

Kulichkov, S.N., 2000. On infrasonic arrivals in the zone of geometric shadow at long distances from surface explosions, in *Proceedings of the Ninth Annual Symposium on Long-Range Propagation,* Oxford, Mississippi, 14–15 September, National Center for Physical Acoustics, pp. 238–251.

Kulichkov, S.N. & Bush, G.A., 2001. Rapid variations in infrasonic signals at long distances from one-type exploisons, *Izv., Atmos. Ocean. Phys.,* **37**(3), 306–313.

Le Pichon, A., Vergoz, J., Blanc, E., Guilbert, J., Ceranna, L., Evers, L. & Brachet, N., 2009. Assessing the performance of the International Monitoring System Infrasound Network: Geographical coverage and temporal variabilities, *J. geophys. Res.,* **114**(D08112), doi:10.1029/2008JD010907.

Le Pichon, A., Blanc, E. & Hauchecorne, A., 2010. *Infrasound Monitoring for Atmospheric Studies,* pp. 735. Springer.

Marcillo, O., Arrowsmith, S., Whitaker, R., Anderson, D., Nippress, A., Green, D. & Drob, D., 2014. Using physics-based priors in a Bayesian algorithm to enhance infrasound source location, *Geophys. J. Int.,* **196**(1), 375–385.

Modrak, R.T., Arrowsmith, S.J. & Anderson, D.N., 2010. A Bayesian framework for infrasound location, *Geophys. J. Int.,* **181,** 399–405.

Negraru, P.T., 2010. Application of seismo-acoustic signals to the study of local site effects, *Acta Geophys.,* **58**(6), 1021–1039.

Rind, D., 1978. Investigation of the lower thermosphere results of ten years of continuous observations with natural infrasound, *J. Atmos. Terr. Phys.,* **40**(10-11), 1199–1209.

Stump, B. *et al.*, 2007. Seismic and infrasound energy generation propagation at local and regional distances: phase I—divine strake experiment. AFRL-RV-HA-TR-2007-1188, available at: http://www.dtic.mil/dtic/tr/fulltext/u2/a480216.pdf, last accessed 2014 February 26.

Suckale, J., Rondenay, S., Sachpazi, M., Charalampakis, M., Hosa, A. & Royden, L.H., 2009. High-resolution seismic imaging of the Western Hellenic Subduction Zone using teleseismic scattered waves, *Geophys. J. Int.,* **178**(2), 775–791.

Vernon, F.L., Hedlin, M.A., Busby, R.W. & Woodward, R., 2010. Observing Infrasound and atmospheric pressure with the NSF EarthScope USArray, Abstract S11A-1920 presented at *2010 Fall Meeting,* AGU, San Francisco, CA, 2010 13–17 December.

Walker, K.T., Shelby, R., Hedlin, M.A.H. & de Groot-Hedlin, C., 2011. Western U.S Infrasonic Catalog: illuminating infrasonic hot spots with the USArray, *J. geophys. Res.,* **116**(B12305), doi:10.1029/2011JB008579.

Wessel, P. & Smith, W.H.F., 1998. New improved version of the generic mapping tools released, *EOS, Trans. Am. geophys. Un,* **79**(49), 579.

Whitaker, R.W. & Mutschlecner, J.P., 2008. A comparison of infrasound signals refracted from stratospheric and thermospheric altitudes, *J. geophys. Res.,* **113**(D08117), doi:10.1029/2007JD008852.

SUPPORTING INFORMATION

Additional Supporting Information may be found in the online version of this article:

Infrasound_array_data.xls
Seismic_USArray_data.xls
summer_celerity data.txt
TTmodel_table.txt
figureS.1.pdf
Infrasound_array_data.xls
(http://gji.oxfordjournals.org/lookup/suppl/doi:10.1093/gji/ggu049/-/DC1).

Please note: Oxford University Press is not responsible for the content or functionality of any supporting materials supplied by the authors. Any queries (other than missing material) should be directed to the corresponding author for the article.